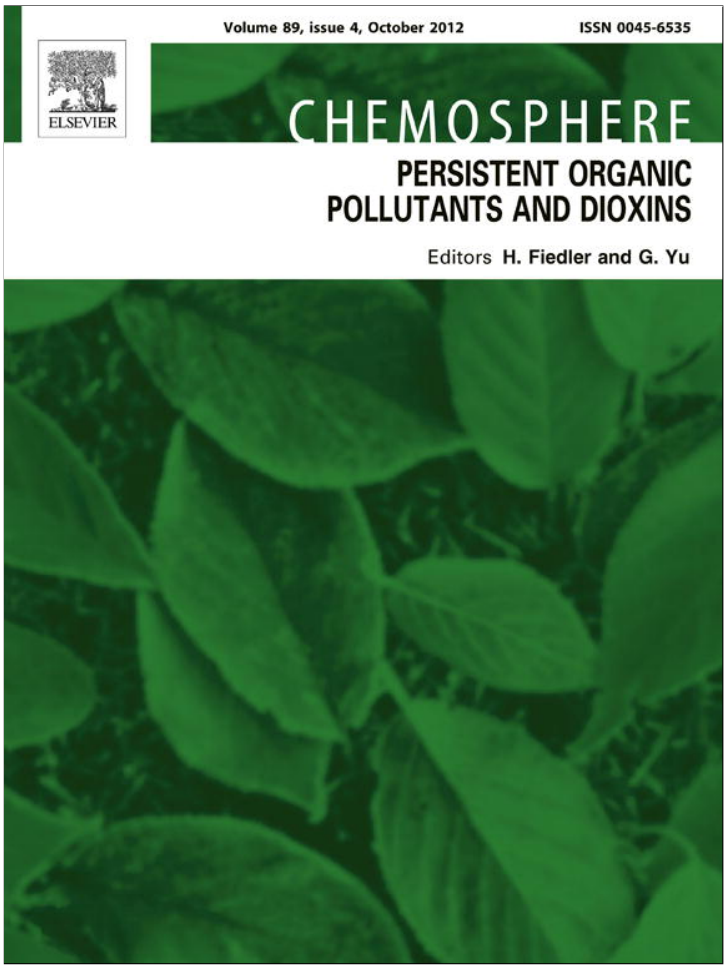

Chemosphere 89 (2012) 389–397

Contents lists available at SciVerse ScienceDirect

Chemosphere

journal homepage: www.elsevier.com/locate/chemosphere

A numerical study on the seasonal variability of polychlorinated biphenyls from the atmosphere in the East China Sea

Jun Ono [a,b,*], Daisuke Takahashi [c], Xinyu Guo [d], Shin Takahashi [d], Hidetaka Takeoka [d]

[a] Graduate School of Frontier Sciences, The University of Tokyo, Kashiwa, Japan
[b] National Institute of Polar Research, Tachikawa, Japan
[c] Hokkaido National Fisheries Research Institute, Fisheries Research Agency, Kushiro, Japan
[d] Center for Marine Environmental Studies, Ehime University, Matsuyama, Japan

HIGHLIGHTS

- We developed a three-dimensional transport model for POPs.
- We applied it to PCB 153 in the East China Sea for the first time.
- PCB 153 concentration is high in winter and low in summer.
- The seasonal variation is mainly controlled by water temperature.
- Horizontal advection and vertical sinking are important for mass balance of PCB 153.

ARTICLE INFO

Article history:
Received 21 November 2011
Received in revised form 14 April 2012
Accepted 19 May 2012
Available online 28 June 2012

Keywords:
Persistent organic pollutants
Three-dimensional transport model
East China Sea
Polychlorinated biphenyls
Seasonal variability
Henry's law constant

ABSTRACT

A three-dimensional/high-resolution transport model for persistent organic pollutants (POPs) has been developed for the East China Sea (ECS). The POPs model has four compartments (gaseous, dissolved, phytoplankton-bound, and detritus-bound phases) and includes processes for diffusive air–water exchange, phytoplankton uptake/depuration to POPs, decomposition of dissolved phase, vertical sinking of phytoplankton, detritus production by phytoplankton mortality, and vertical sinking and decomposition of detritus. The POPs model is coupled with an ocean circulation model that can reproduce the seasonal variation in physical variables to represent the advection and diffusion of POPs. We applied the POPs model to the polychlorinated biphenyl congener 153 (PCB 153) from the atmosphere and examined the behavior of PCB 153 in the ocean. The model showed a remarkable seasonal variability of PCB 153. Concentrations in the dissolved and particulate phases are high in winter (January–March) and low in summer (July–September). In coastal regions, where chlorophyll *a* concentration is high, horizontal and vertical distributions in the dissolved and particulate PCB 153 concentrations are strongly affected by phytoplankton uptake. The sensitivity experiments on the dynamics of PCB 153 suggested that a change of Henry's law constant associated with water temperature is the major factor controlling the seasonal variability of PCB 153. The model-based yearly mass balance of PCB 153 in the ECS indicated that most of the atmospheric input (35.5 kg year^{-1}) is removed by the horizontal advection outside the ECS (19.0 kg year^{-1}) and accumulates to the sea bottom by vertical sinking (15.7 kg year^{-1}). For comparison with PCB 153, we also conducted simulations for PCB 52, 101, and 180. The seasonal variations are similar to that of PCB 153. The mass balance of PCB 52 that has short half-life time and less hydrophobic property shows the different results compared with PCB 101, 153, and 180.

1. Introduction

Global contamination by persistent organic pollutants (POPs) such as hexachlorocyclohexanes (HCHs), dichloro diphenyl trichloroethanes (DDTs), and polychlorinated biphenyls (PCBs) and their impacts on wildlife and ecosystems have been of concern over the last decade. POPs are mainly characterized by their persistence, long-range transport in the atmosphere and the ocean, bioaccumulation, and toxicity. Thus, understanding and quantifying the dynamics of POPs are important to assess their environmental impact and final fate. In particular, the ocean is considered to be the one of the global POPs reservoirs (Tanabe and Tatsukawa, 1983; Iwata et al., 1993), although it may not be as high as the soil

* Corresponding author at: Graduate School of Frontier Sciences, The University of Tokyo, 5-1-5, Kashiwanoha, Kashiwa, Chiba 277-8561, Japan. Tel./fax: +81 4 7136 4122.
E-mail address: jo@1.k.u-tokyo.ac.jp (J. Ono).

0045-6535/$ - see front matter © 2012 Elsevier Ltd. All rights reserved.
http://dx.doi.org/10.1016/j.chemosphere.2012.05.049

reservoir (Jurado et al., 2004; Lohmann et al., 2007). From observations in the open ocean, Tanabe and Tatsukawa (1983) showed that the vertical distribution of PCBs and DDTs are almost homogeneous and suggested that PCBs and DDTs are rapidly and abundantly transported by sinking particles. Lohmann et al. (2006) reported that PCBs in the surface ocean are transported to the deep ocean in association with deep water formation. These studies imply that the deep ocean can be a candidate for the ultimate fate of many POPs.

POPs emitted into the atmosphere can be transported to remote areas and be deposited to the ocean by diffusive air–water exchange flux, dry deposition, or wet deposition in rain or snow. The dissolved POPs are absorbed by the phytoplankton in the surface ocean, and then are transported to the deep ocean by vertical sinking of the particle-bound POPs, and finally accumulated to the sea bottom. POPs in the sediment may be brought back into the water column by resuspension. The behaviors of POPs in the ocean are complex as mentioned above. To describe and understand the complex three-dimensional dynamics of POPs in the ocean and to predict fate of POPs in the ocean, a numerical model is a useful tool. Numerical modeling studies suggest that not only horizontal advection and diffusion by current and turbulence but also vertical transport of POPs absorbed into phytoplankton are important processes (Wania et al., 1998; Dachs et al., 1999).

So far, most numerical modeling of POPs in the ocean has been based on a box model (Dachs et al., 1999, 2000, 2002). Using the box model for air–water–phytoplankton exchanges, Dachs et al. (1999) showed that air–water exchange is influenced by phytoplankton biomass and growth rate. Wania et al. (2001) and Breivik and Wania (2002) evaluated mass balance for PCBs and HCH in the Baltic Sea, respectively, using a multimedia mass balance model. Jurado et al. (2007) developed a one-dimensional dynamic coupled hydrodynamic-contaminant model and applied it to a Mediterranean continental shelf environment. In addition, Meijer et al. (2006, 2009) developed a dynamic flux model describing POPs fate and cycling in lakes and assessed the role of internal biogeochemical cycling with respect to accumulation of four different PCBs.

On the other hand, numerical studies of POPs using a three-dimensional model including advection and diffusion processes have been also reported. Schenker et al. (2008) evaluated a global environmental fate model for DDTs, which are representative hydrophobic POPs, by a comparison with the field measurements. They documented that good agreement between the model and measurements in the soil and air compartment but not in ocean water, and suggested high variability of DDTs concentrations and various reactions in the ocean including the removal process to deep water as possible factors for such discrepancy between the model and measurements. Recently, Guglielmo et al. (2009) developed a global three-dimensional atmosphere–ocean general circulation model with a marine carbon cycle model (MPI-MCTM) and Kawai et al. (2009) developed a Finely-Advanced Transboundary Environmental model. Stemmler and Lammel (2009, 2010) examined the global dynamics for γ-HCH, DDT, PCBs, and PFOA using MPI-MCTM. Their studies paid attention to POPs dynamics in the global scale and showed very interesting and important results. Furthermore, Guglielmo et al. (2012) studied the global fate and transport of γ-HCH and DDT using MPI-MCTM with and without the sea ice dynamics.

With respect to the regional POPs modeling, Ilyina et al. (2006, 2008) has developed a three-dimensional transport model for POPs and investigated the fate of γ-HCH, α-HCH, and PCB 153 in the North Sea. However, the POPs modeling has not yet been studied in the East Asia, where the environmental contamination by POPs still continues even now. In particular, the East China Sea (ECS) (Fig. 1a), including the Yellow and Bohai Seas, is surrounded by highly industrialized areas of the East Asian countries, which can be potential sources of POPs. In fact, monitoring studies of POPs using fishes have shown that POPs concentration in the ECS was high (Ueno et al., 2003). However, the detailed dynamics of POPs in the ECS has not yet been understood well.

In this study, we developed a three-dimensional POPs model and applied it to the ECS for the first time. The objective in this study is to investigate the key process affecting POPs dynamics in the ECS, particularly focusing on the seasonal variability in PCB 153 from the atmosphere as a first step toward the realistic numerical simulation of POPs. The rest of this paper is as follows. Section 2 describes a three-dimensional/high-resolution transport model for POPs in the ECS. In Section 3, we present results from numerical simulations applied to PCB 153 and its mass balance, and then discuss the results of a series of numerical experiments designed to investigate the effects of water temperature, wind speed, chlorophyll *a*, seasonal variation in the gaseous POPs, sinking velocity of particles, and mortality rate on the behavior of the POPs in the ECS. Section 4 makes some concluding remarks.

2. Model description

2.1. POPs transport model

To incorporate the effects of advection and diffusion of POPs by currents and turbulence, we used a three-dimensional ocean circulation model in the ECS (Guo et al., 2003), which is based on the Princeton Ocean Model (POM) (Blumberg and Mellor, 1987; Mellor, 2003). This model can well reproduce seasonal variation in the physical fields of the ECS. The model domain and bathymetry, covering the Bohai Sea, Yellow Sea, and ECS, are shown in Fig. 1a. The grid in this model has a resolution of 1/18° (~5 km on average) horizontally and 21 sigma (a vertical coordinate scaled by the water column depth with 0 at sea surface and −1 at sea bottom) levels vertically (0.000, −0.002, −0.004, −0.010, −0.020, −0.040, −0.060, −0.080, −0.100, −0.120, −0.140, −0.170, −0.200, −0.300, −0.400, −0.500, −0.650, −0.800, −0.900, −0.950, −1.000).

Our POPs transport model includes four compartments: gaseous POPs (C_A), dissolved POPs (C_W), phytoplankton-bound POPs (C_{WP}), and detritus-bound POPs (C_{WD}). As for C_{WP}, we considered it as the sum of the concentrations in the phytoplankton surface (C_{WPS}) and matrix (C_{WPM}), according to Dachs et al. (1999). The three-dimensional equations describing the transport of POPs for each compartment in the ocean are given by following equations

$$\frac{\partial C_W}{\partial t}+u\frac{\partial C_W}{\partial x}+v\frac{\partial C_W}{\partial y}+w\frac{\partial C_W}{\partial z}=\frac{\partial}{\partial z}\left(K_h\frac{\partial C_W}{\partial z}\right)+F_C(C_W)+B_I(C_W), \tag{1}$$

$$\frac{\partial C_{WPS}}{\partial t}+u\frac{\partial C_{WPS}}{\partial x}+v\frac{\partial C_{WPS}}{\partial y}+(w+w_{sp})\frac{\partial C_{WPS}}{\partial z}=\frac{\partial}{\partial z}\left(K_h\frac{\partial C_{WPS}}{\partial z}\right)+F_C(C_{WPS})+B_I(C_{WPS}), \tag{2}$$

$$\frac{\partial C_{WPM}}{\partial t}+u\frac{\partial C_{WPM}}{\partial x}+v\frac{\partial C_{WPM}}{\partial y}+(w+w_{sp})\frac{\partial C_{WPM}}{\partial z}=\frac{\partial}{\partial z}\left(K_h\frac{\partial C_{WPM}}{\partial z}\right)+F_C(C_{WPM})+B_I(C_{WPM}), \tag{3}$$

$$\frac{\partial C_{WD}}{\partial t}+u\frac{\partial C_{WD}}{\partial x}+v\frac{\partial C_{WD}}{\partial y}+(w+w_{sd})\frac{\partial C_{WD}}{\partial z}=\frac{\partial}{\partial z}\left(K_h\frac{\partial C_{WD}}{\partial z}\right)+F_C(C_{WD})+B_I(C_{WD}) \tag{4}$$

Here C_W, C_{WPS}, C_{WPM}, and C_{WD} are concentrations (pg m^{-3}); t is time (s); x, y, and z are the zonal, meridional and vertical coordinates

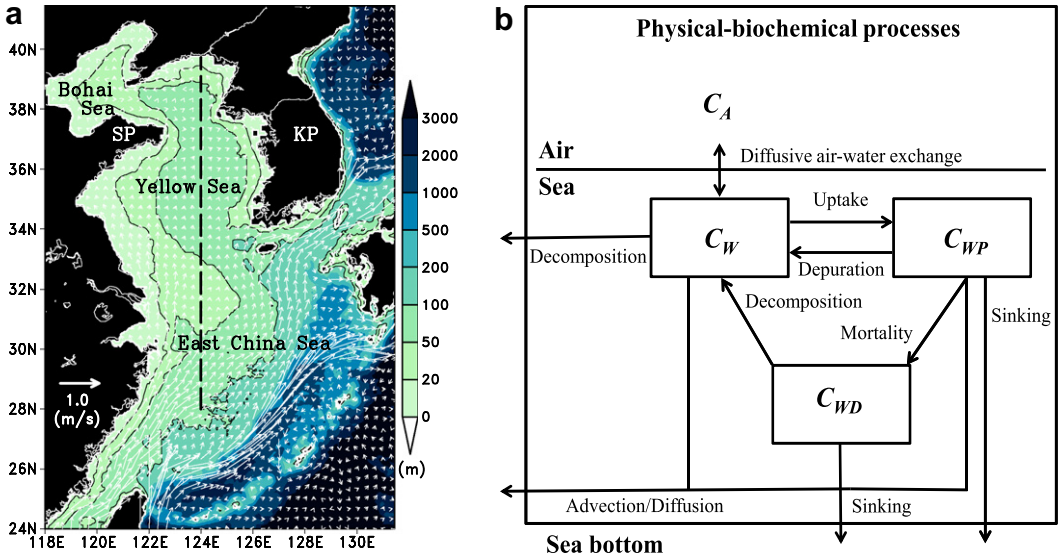

Fig. 1. (a) Model domain and bathymetry. Monthly averaged surface current in August is superimposed by vectors. The 20, 50, and 100 m isobaths are also superimposed by solid lines. A dashed line denotes the section along which vertical structures of PCB 153 are presented in Figs. 5 and 6. SP and KP denote the Shandong and Korean Peninsulas. (b) Schematics of physical–biochemical processes for POPs. The POPs model includes four compartments: gaseous POPs (C_A), dissolved POPs (C_W), phytoplankton-bound POPs (C_{WP}), and detritus-bound POPs (C_{WD}). See text for detailed explanations on the physical–biochemical processes.

(m); u, v, and w are their velocity components (m s^{-1}); w_{sp} and w_{sd} represent the sinking velocity (m s^{-1}) of phytoplankton or detritus (see Appendix A in Supplementary material); K_h is the vertical eddy diffusivity coefficient (m^2 s^{-1}) calculated by a 2.5 Mellor–Yamada turbulence closure scheme (Mellor and Yamada, 1982); $F_C(C_W)$, $F_C(C_{WPS})$, $F_C(C_{WPM})$, and $F_C(C_{WD})$ are the horizontal diffusion terms parameterized according to the Smagorinsky diffusion scheme (Smagorinsky, 1963); and $B_I(C_W)$, $B_I(C_{WPS})$, $B_I(C_{WPM})$, and $B_I(C_{WD})$ are the biochemical processes for each compartment and will be described in Appendix A in Supplementary material. The model numerical scheme is similar to that used for solving variables such as salinity and temperature in POM. The variables at z-levels are converted to those at sigma coordinates in the model. The integration of Eqs. (1)–(4) is carried out by two steps. The first step is to explicitly integrate C_W, C_{WPS}, C_{WPM}, and C_{WD} for advection and horizontal diffusion. The second step is to implicitly solve C_W, C_{WPS}, C_{WPM}, and C_{WD} for vertical diffusion. A first-order upstream scheme (Smolarkiewicz, 1984) was used for advection in Eqs. (1)–(4).

2.2. Biochemical processes for POPs

Fig. 1b shows the schematics of physical–biochemical processes for POPs. In the ocean, a proportion of the dissolved POPs is absorbed by the surface and matrix of phytoplankton while some are decomposed. Phytoplankton-bound POPs are affected by three processes: uptake/depulation, natural mortality, and vertical sinking of phytoplankton. The natural mortality of phytoplankton transforms phytoplankton-bound POPs into detritus-bound POPs. Some detritus-bound POPs are transported to the deep ocean by vertical sinking of detritus, and others are transformed into dissolved POPs by decomposition of detritus. In the present POPs modeling, we did not include processes on the dissolved organic matter, zooplankton, river discharge, sediments and so on, although these processes are important for POPs dynamics (e.g., Guglielmo et al., 2009; Stemmler and Lammel, 2009; Meijer et al., 2009; Berrojalbiz et al., 2009). These processes have not been well understood in the ECS due to the lack of data. Therefore, as a first step of our POPs modeling, we focus on the physical–biochemical processes shown in Fig. 1b and leave these processes as future works. The biochemical processes B_I in Eqs. (1)–(4) for C_W, C_{WPS}, C_{WPM}, and C_{WD} are given in Appendix A in Supplementary material.

2.3. Model setup

In the present study, gaseous POPs concentration (C_A) is supplied to the ocean via the diffusive air–water exchange flux. We did not take into account dry and wet particle deposition because few observations are available for these two processes in the ECS. In addition, Jurado et al. (2005) estimated the dominant deposition process for the global oceans and showed that PCBs are primarily introduced into the ocean by the diffusive air–waver exchange flux almost everywhere. The surface boundary condition for dissolved POPs concentration (C_W) is therefore expressed as

$$K_h \frac{\partial C_W}{\partial z} = F_{AW}, \tag{5}$$

where F_{AW} (pg m^{-2} s^{-1}) is the net flux of POPs between air and water. Following Bidleman and McConnell (1995), F_{AW} is given by

$$F_{AW} = k_{AW}\left(C_W - \frac{C_A}{H'}\right), \tag{6}$$

where H' is the dimensionless Henry's law constant corrected for water temperature (Bamford et al., 2000, 2002), and k_{AW} (m s^{-1}) is the mass transfer velocity between air and water. To calculate k_{AW}, we used wind speed data from the European Remote-Sensing satellites ERS–1 and ERS–2. Since the net flux of POPs between air and water is affected by wind speed and water temperature, their spatial distributions in February and August, as examples, are given in Appendix B.1 in Supplementary material. The other specific parameters and equations used in the air–water exchange process are summarized in Supplementary Table 3.

The target compound of POPs is polychlorinated biphenyls congener 153 (PCB 153) with the more hydrophobic characteristic. The gaseous PCB 153 concentration was assumed to be horizontally uniform throughout the year and set to 2.08 pg m^{-3}, which was calculated on the basis of data from Jaward et al. (2005). In the initial and open boundary conditions, the dissolved PCB 153 concentration, the phytoplankton-bound PCB 153 concentration, and

the detritus-bound PCB 153 concentration were set to 0 pg m^{-3}. Consequently, the PCB 153 in our results has a single source, i.e., from the atmosphere. The model was integrated for 5 years and the last year was analyzed. This result will be referred to hereinafter as the control-run.

For comparison with other PCB congener, we also conducted simulations for PCB 52, 101, and 180.

3. Results and discussion

The monthly means of dissolved PCB 153 concentration (C_W) and particulate PCB 153 concentration ($C_{WP} + C_{WD}$), both averaged over the whole volume of the model domain, that of surface flux (F_{AW} in Eq. (6)) averaged over the whole surface area of the model domain, and that of sinking flux ($[w + w_{sp}]C_{WP} + [w + w_{sd}]C_{WD}$ in the deepest sigma layer.) averaged over the whole bottom area of the model domain present clear seasonal variability (Fig. 2). Concentrations in the dissolved and particulate PCB 153 and surface and sinking fluxes are all high in winter (January–March) and low in summer (July–September). There is a one month time lag between monthly surface flux and monthly dissolved PCB 153 concentration. The surface flux reaches a maximum (minimum) in January (August), while the dissolved PCB 153 concentration becomes maximum (minimum) one month later. The similar seasonal variation can also be seen in the results of PCB 52, 101, and 180, while their amplites are different (see Appendix B.4 of Supplementary material for detailed explanations).

3.1. Horizontal and vertical structures of PCB 153

To examine the horizontal structures of PCB 153 in summer and winter, horizontal distributions of surface flux and surface concentrations in the dissolved and particulate PCB 153 in February and August are shown in Fig. 3. The surface flux by diffusive air–water exchange is higher in February than in August (Fig. 3a and b). The highest surface flux area in February is mainly formed in coastal regions from China to the Korean Peninsula (Fig. 3a). Associated with the high surface flux, surface concentrations of dissolved and particulate PCB 153 were also higher in February (Fig. 3c and e) than in August (Fig. 3d and f). Interestingly, in coastal regions, where the surface chlorophyll *a* concentration is highest (see Supplementary Fig. 1a), the surface dissolved PCB 153 concentration is lower there than in offshore regions (Fig. 3c). In contrast, the surface particulate PCB 153 concentration is higher in coastal regions than in offshore regions (Fig. 3e). In coastal regions, the dissolved PCB 153 is absorbed by phytoplankton and converted to particulate PCB 153. On the other hand, the surface flux in August is small (Fig. 3b) and the dissolved and particulate PCB 153 concentrations are also low (Fig. 3d and f). In the central Yellow Sea, the surface flux becomes negative, indicating possible release of PCB153 from the sea to the air. The negative surface flux in summer is caused by the high surface water temperature in the central Yellow Sea that induces the volatilization of PCB 153 from the surface ocean (Fig. 3b).

Fig. 4 shows bottom concentrations in dissolved and particulate PCB 153 and the sinking flux in February and August. In February, the bottom dissolved (Fig. 4a) and bottom particulate (Fig. 4c) PCB 153 concentrations are high near the coast. In particular, the bottom dissolved PCB 153 concentration is high around the southern part of the Shandong Peninsula, along the coast from 25 to 30 °N in China, and in the Yellow Sea. As a result, the sinking flux of particulate PCB 153 also becomes large in these coastal regions (Fig. 4e). The bottom dissolved PCB 153 concentration is high in the Yellow Sea in August (Fig. 4b), and even higher in February. With the evolution of the mixed layer in winter (January–March), a large

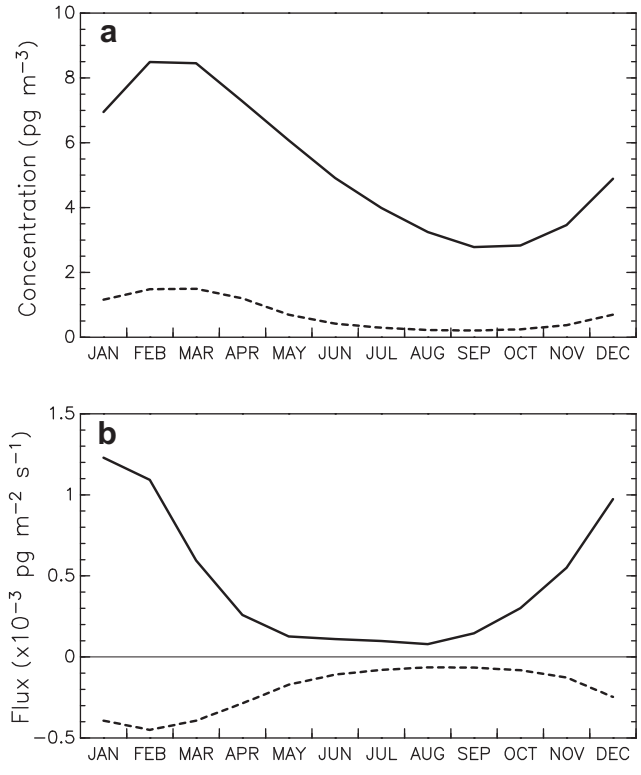

Fig. 2. Time series of monthly averaged (a) dissolved (solid line) and particulate (dashed line) PCB 153 concentrations, and (b) the surface flux of PCB 153 from the atmosphere to the ocean (solid line) and the sinking flux of PCB 153 from the water column to the sea bottom (dashed line), averaged over the whole area of the East China Sea.

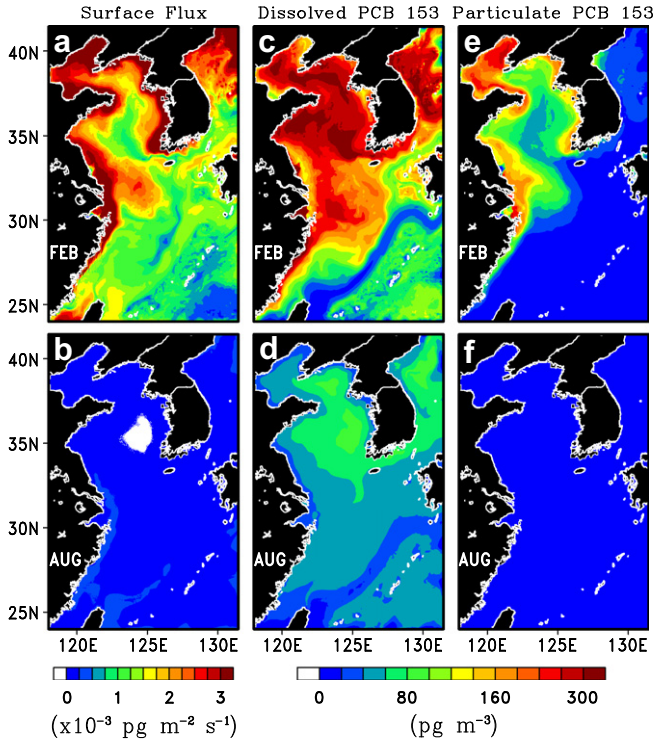

Fig. 3. Horizontal distributions of simulated results in February and August. (a and b) Surface flux of PCB 153 from the atmosphere to the ocean, (c and d) dissolved PCB 153 concentrations at the surface, and (e and f) particulate PCB 153 concentrations at the surface.

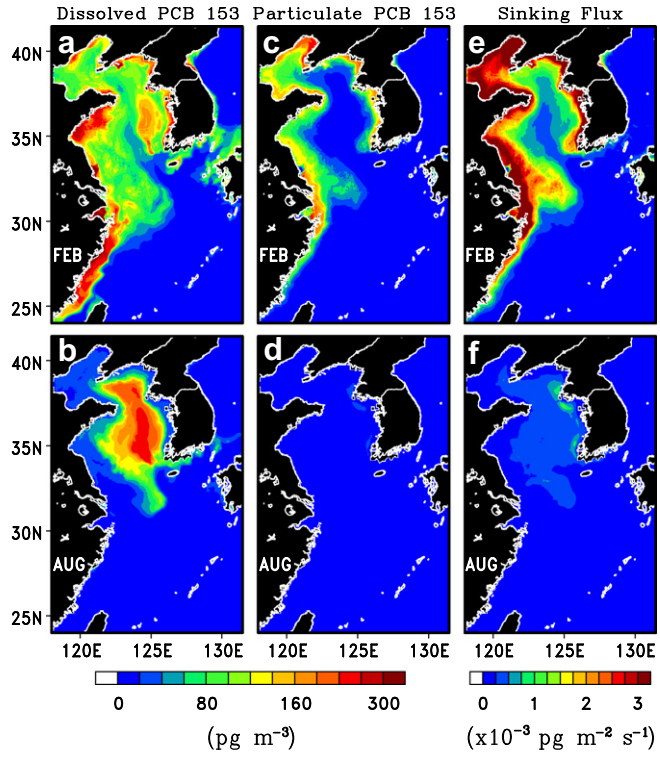

Fig. 4. Horizontal distributions of simulated results in February and August. (a and b) Dissolved PCB 153 concentration at the bottom, (c and d) particulate PCB 153 concentrations at the bottom, and (e and f) sinking flux of PCB 153 to the bottom.

amount of PCB 153 must be transported to the bottom layer. However, this process cannot induce a higher bottom concentration of dissolved PCB 153 in summer than in winter. Another important factor is the development of strong stratification from spring to summer in the central Yellow Sea. The presence of strong stratification in summer prevents not only the vertical transfer of heat from the sea surface to the sea bottom that induces the formation of cold bottom water, i.e., the well-known Yellow Sea Cold Water (e.g., Park et al., 2011), but also the vertical transfer of dissolved PCB 153. The combination of the latter and the decomposition of particulate PCB 153 attached to phytoplankton and detritus whose sinking is not affected by the stratification induces the accumulation of dissolved PCB 153 in the bottom layer of the central Yellow Sea. The low concentration of bottom particulate PCB 153 (Fig. 4d) and low sinking flux (Fig. 4f) also supports the decomposition of particulate PCB 153 in the bottom layer.

To examine the vertical structure of PCB 153 along a section from the Yellow Sea to the East China Sea, the vertical distribution of dissolved and particulate PCB 153 concentrations, together with some physical and biological variables, at 124°E in February and August are presented in Figs. 5 and 6, respectively. In February, the horizontal variation in surface flux of PCB 153 along the section (Fig. 5b) generally corresponds to that of chlorophyll *a* (Fig. 5a), which is high in regions offshore of the Changjiang River mouth and in coastal regions of the Yellow Sea. Corresponding to the surface flux, the dissolved PCB 153 concentration is also high. It has a strong vertical variation, being generally high at the surface but low at the bottom, which is different from the vertically homogeneous water temperature. Such vertical variation in the dissolved concentration is formed by the high surface flux. On the other hand, there is also an apparent horizontal variation in the dissolved PCB 153 (Fig. 5d). The behavior of dissolved PCB 153 is thus affected not only by physical processes but also biological processes. The dissolved PCB 153 is absorbed by the abundant phytoplankton in regions, where surface chlorophyll *a* concentration is high (Fig. 5a and d), and then it is changed into particulate PCB 153 (Fig. 5d and e). As a consequence, low dissolved PCB 153 corresponds to high particulate PCB 153 (Fig. 5d and e) and the sinking flux by vertical sinking of particulate PCB 153 is also high in these regions (Fig. 5b).

In August, the wind becomes weak (Fig. 6a) and the sea surface water temperature becomes high (Fig. 6c) but the surface chlorophyll *a* concentration changes little (Fig. 6a). The dissolved PCB 153 concentration is locally high in the middle and bottom layers of the Yellow Sea (Fig. 6d), while that in the surface layer is low due to the small surface flux (Fig. 6b). The high concentration area is consistent with regions of low temperature, i.e., the Yellow Sea Cold Water. This suggests that the bottom regions of the Yellow Sea become the reservoir of POPs such as PCBs. The particulate PCB 153 concentration is also high in the middle layer but is only about half that in February. As a result, the sinking flux also becomes low (Fig. 6b).

3.2. Mass balance of PCB 153 in the East China Sea

To elucidate the important processes affecting the behavior of PCB 153 in the ocean, a mass balance of PCB 153 in the ECS was calculated using the simulated result for the control-run (Fig. 7). The yearly averaged biomass of PCB 153 integrated over the whole volume of the model domain was calculated as follows:

$$\frac{\int_1^{365} \iiint C(x,y,z,t)\,dx\,dy\,dz\,dt}{\int_1^{365} dt}, \tag{7}$$

where C is PCB 153 concentration (kg m^{-3}) that is function of space (x,y,z) and time (t); dx, dy, dz are unit distance (m) in three directions of space; dt is a unit time (day). The value was estimated to be 7.1, 0.9, and 0.1 kg, for dissolved PCB 153, phytoplankton-bound PCB 153, and detritus-bound PCB 153, respectively. Most PCB 153 in the ocean has been found to be dissolved PCB 153 (~87%). The yearly integrated PCB 153 from the atmosphere into the ocean is estimated to be 35.5 kg year^{-1}. Of the dissolved PCB 153, 18.1 kg year^{-1} is removed by horizontal advection outside the ECS and 18.3 kg year^{-1} is absorbed by phytoplankton, while 0.5 kg year^{-1} is decomposed. 7.0 kg year^{-1} of phytoplankton-bound PCB 153 is transformed into detritus-bound PCB 153 through the mortality process. Most of the particulate PCB 153 ($C_{WP} + C_{WD}$) is deposited to the sea bottom by vertical sinking (15.7 kg year^{-1}), while advection (0.9 kg year^{-1}) of particulate PCB 153 and decomposition (1.7 kg year^{-1}) of detritus-bound PCB 153 are not significant processes for the mass balance.

Our results for the mass balance of PCB 153 in the whole ECS is summarized as follows: the atmospheric input is 35.5 kg year^{-1}, among which 19 kg (54%) is removed by horizontal advection of dissolved and particulate PCB 153 outside the ECS and 15.7 kg (45%) is accumulated to the sea bottom by vertical sinking of particulate PCB 153. In the cases of PCB 101 and 180, most of the atmospheric input is also removed by horizontal advection and sinking flux. However, in the case of PCB 52, decomposition of the dissolved phase and advection are larger and sinking flux is smaller than those in the PCB 101, 153, and 180 (see the Appendix B.4 of Supplementary material for detailed explanations).

3.3. Key process responsible for seasonal variability in PCB 153

To clarify the key process responsible for the seasonal variability in PCB 153, we performed three sensitivity experiments, a chlorophyll-run, wind-run, and temperature-run, as described in Appendix B.2 in Supplementary material and compared the calculated monthly volume-averaged dissolved and particulate PCB 153

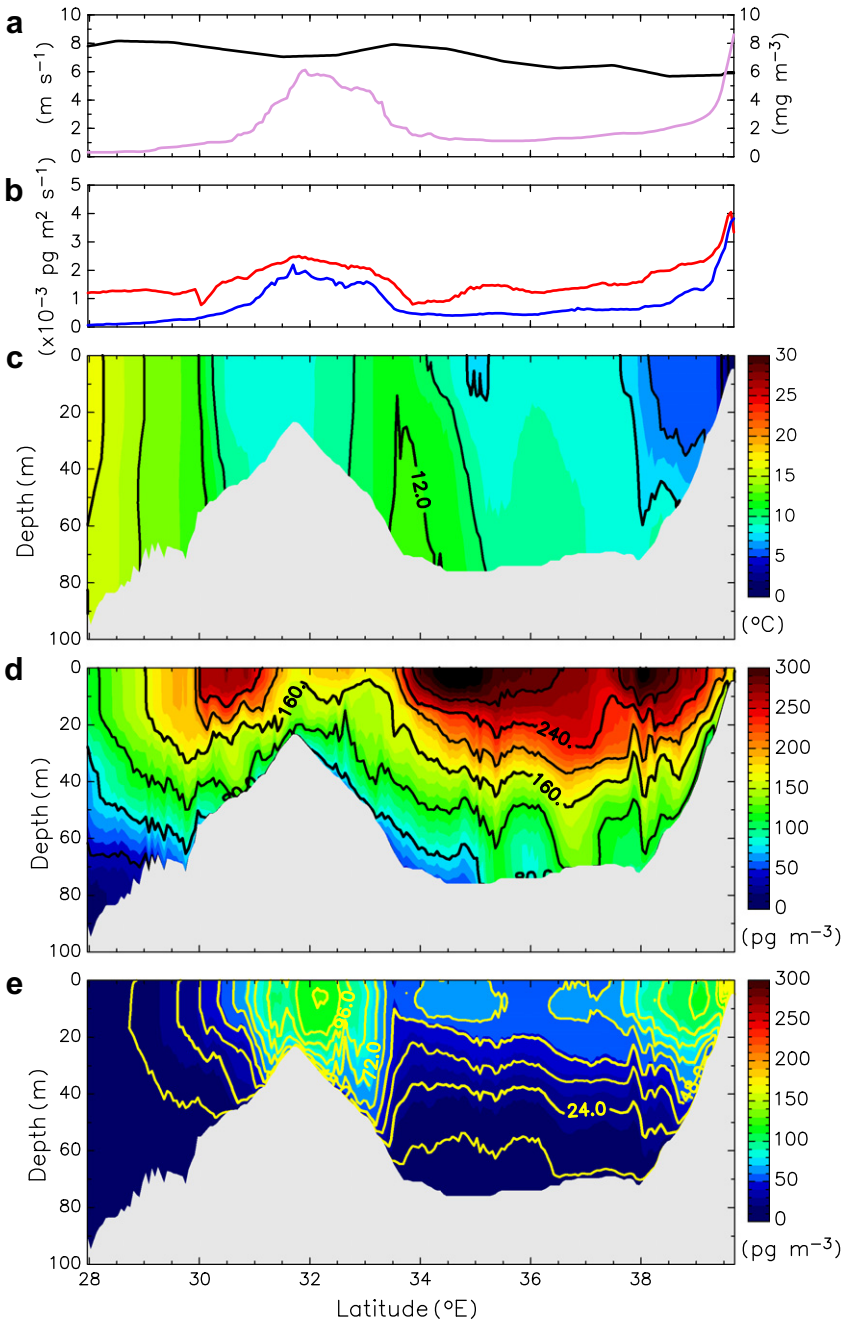

Fig. 5. Distributions of (a) wind speed (black) and surface chlorophyll *a* concentration (purple), (b) surface flux of PCB 153 from the atmosphere to the ocean (red) and sinking flux of PCB 153 (blue), (c) water temperature, and (d) dissolved and (e) particulate PCB 153 concentrations along the section shown in Fig. 1a, in February. Contour intervals are 2.0 °C for water temperature, 40 pg m^{-3} for dissolved PCB 153, and 12 pg m^{-3} for particulate PCB 153. (For interpretation of the references to colour in this figure legend, the reader is referred to the web version of this article.)

with those from the control-run (Supplementary Fig. 2). The seasonal cycle in PCB 153 in the chlorophyll-run is almost the same as that in the control-run. However, the dissolved PCB 153 concentration increases somewhat in February–April, while the particulate PCB 153 concentration decreases. This may be partly because the yearly averaged chlorophyll *a* concentration used in the chlorophyll-run is lower than the chlorophyll *a* concentration in February–April used in the control-run. The seasonal cycle in PCB 153 is also present in the wind-run but the maximum value in winter becomes smaller than that in the control-run. In the temperature-run, the seasonal cycle in PCB 153 is significantly different from that in the control-run and the maximum value in winter becomes smallest of all sensitivity experiments, indicating that water temperature likely play the most important role in determining the maximum values of dissolved and particulate PCB 153 in winter. On the other hand, the minimum values of dissolved and particulate PCB 153 are not sensitive to changes in wind speed, water temperature, and chlorophyll *a* concentration.

Here we discuss these the mechanisms in more detail. In the present study, we have taken account only gaseous PCB 153 from the atmosphere through the diffusive air–water exchange flux. As shown in Eq. (6), the net flux of PCB 153 between air and water depends on the mass transfer velocity (k_{AW}), dissolved PCB 153 concentration (C_W), gaseous PCB 153 concentration (C_A), and

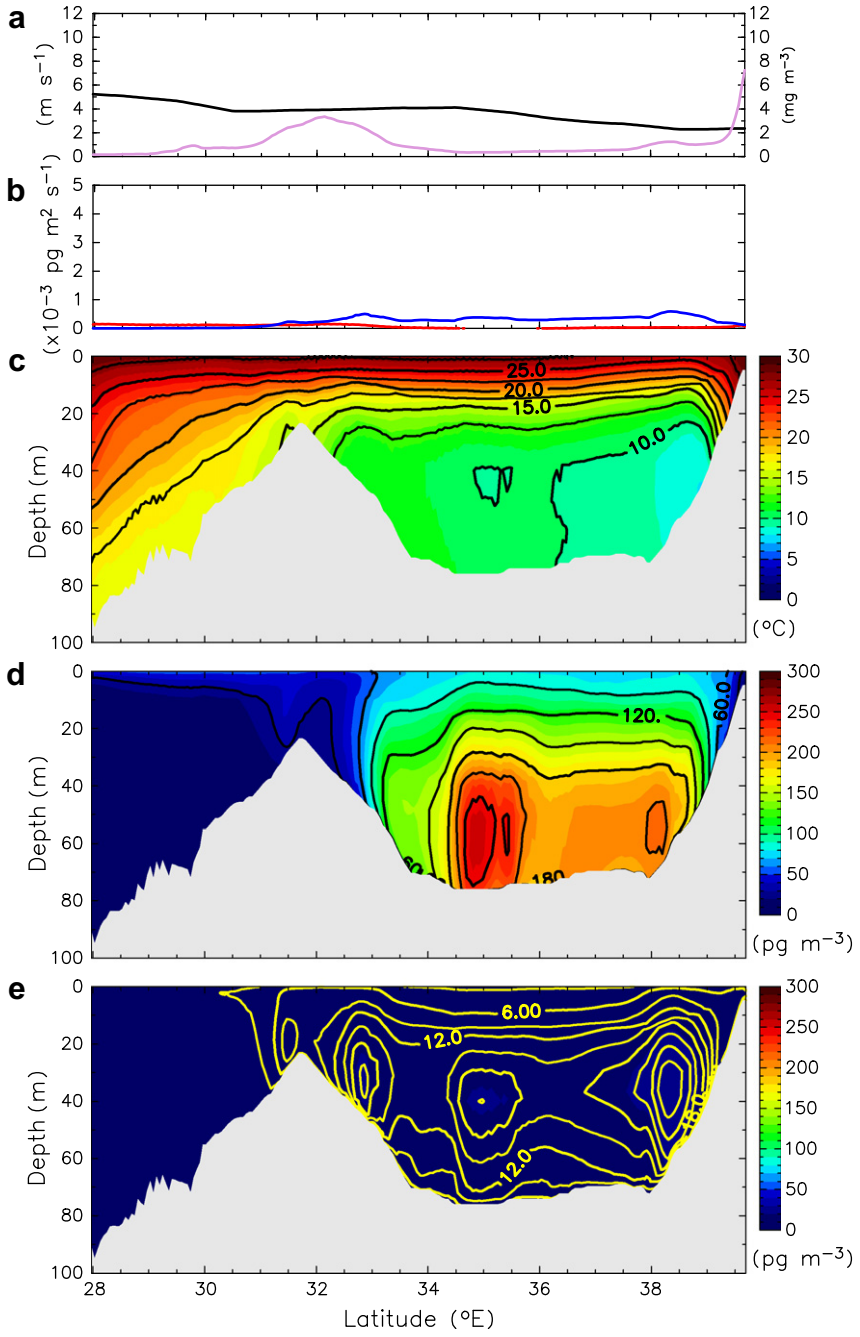

Fig. 6. Similar to Fig. 5, but for August. Contour intervals are 2.5 °C for water temperature, 30 pg m^{-3} for dissolved PCB 153, and 3 pg m^{-3} for particulate PCB 153.

Henry's law constant (H'). As shown in Supplementary Table 3, Henry's law constant depends closely on water temperature, i.e., low (high) temperature results in a low (high) value of Henry's law constant. Since we use a constant concentration of gaseous PCB 153 throughout the year, the C_A/H' term in Eq. (6) increases in winter and decreases in summer. Consequently, the surface flux from the atmosphere to the ocean becomes large in winter and small in summer. This explains how the seasonal variability in PCB 153 is caused by that in water temperature through Henry's law constant. Since the mass transfer velocities between air and water (k_{AW}) depend on wind speed (Supplementary Table 3), seasonal variability in PCB 153 may be also influenced by that in wind speed. However, the change in Henry's law constant with water temperature is more significant for the seasonal variability of PCB 153 than that in the mass transfer velocities with wind speed. Consequently, the water temperature is the first contributor to the seasonal variability of PCB 153 and the wind speed is secondary, while that of chlorophyll *a* is not so significant.

4. Concluding remarks

On the basis of previous numerical studies (Dachs et al., 1999, 2000, 2002), we newly developed a three-dimensional/high-resolution transport model for POPs and applied it to the ECS for the first time. To investigate the dynamics of PCB 153 from the atmosphere in the ocean, the model was coupled with an ocean circulation model that can well reproduce the velocity fields in the ECS. The model revealed that concentrations of dissolved and particulate PCB 153 exhibit clear seasonal variations with higher values in winter (January–March) and lower values in summer (July–

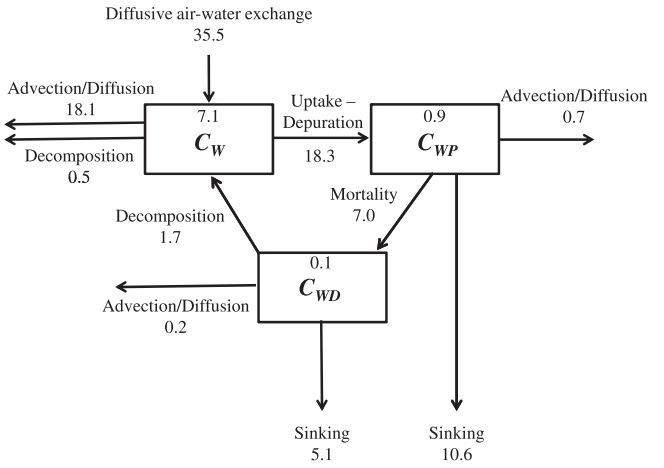

Fig. 7. Yearly integrated mass balances (kg year^{-1}) calculated by the model. Each arrow denotes a physical–biochemical process on PCB 153. The values given above C_W, C_{WP}, and C_{WD} indicate the biomass in each phase.

September). Sensitivity experiments indicate that the seasonal variability of PCB 153 is mainly caused by that of Henry's law constant, which depends closely on water temperature. From the mass balance of PCB 153, most of the atmospheric input (35.5 kg year^{-1}) by diffusive air–water exchange is removed by horizontal advection (19.0 kg year^{-1}) and accumulated to the sea bottom by vertical sinking (15.7 kg year^{-1}).

The present study has focused on the seasonal variability of PCB 153 from the atmosphere by the diffusive air–water flux, as a first step toward realistic simulation of POPs transport. In our study area, however, the Changjiang and Yellow Rivers also carry large amounts of suspended particulate matter (SPM) and freshwater, which can also be sources of POPs. In addition, resuspension of particulate PCB 153 from sediments may be an important process for the behavior of POPs in shallow coastal regions, where wind waves and tidal currents are dominant. Therefore, to adequately represent the behaviors of POPs, our future model should take account of the following processes: (1) river discharge and SPM, (2) resuspension at the sea bottom, (3) temporal and spatial variations of POPs concentration in the atmosphere, (4) POPs concentrations at the open boundaries, and (5) dry and wet deposition. At the same time, continuous POPs monitoring or observations are also needed to quantify POPs impact and to validate the model results.

Acknowledgements

We are grateful to Gan Zhang and Jordi Dachs for their useful discussion and comments. We would like to thank Joji Ishizaka of Nagoya University for providing satellite Chlorophyll *a* data. This study was supported by a Grant-in-Aid for the Global COE Program of Ehime University (Leader: Prof. Shinsuke Tanabe) from the Japanese Ministry of Education, Culture, Sports, Science and Technology.

Appendix A. Supplementary data

Supplementary data associated with this article can be found, in the online version, at http://dx.doi.org/10.1016/j.chemosphere.2012.05.049.

References

Bamford, H.A., Poster, D.L., Baker, J.E., 2000. Henry's law constants of polychlorinated biphenyl congeners and their variation with temperature. J. Chem. Eng. Data 45, 1069–1074.

Bamford, H.A., Poster, D.L., Huie, R.E., Baker, J.E., 2002. Using extrathermodynamic relationships to model the temperature dependence of Henry's law constants of 209 PCB congeners. Environ. Sci. Technol. 34, 4395–4402.

Berrojalbiz, N., Lacorte, S., Calbet, A., Saiz, E., Barata, C., Dachs, J., 2009. Accumulation and cycling of polycyclic aromatic hydrocarbons in zooplankton. Environ. Sci. Technol. 43, 2295–2301.

Bidleman, T.F., McConnell, L.L., 1995. A review of field experiments to determine air–water gas exchange of persistent organic pollutants. Sci. Total Environ. 159, 101–107.

Blumberg, A.F., Mellor, G.L., 1987. A description of a three dimensional coastal ocean circulation model. In: Heaps, N. (Eds.), Three-Dimensional Coastal Ocean Models, Coast. Estuar. Sci., vol. 4, AGU, Washington, DC, pp. 1–16.

Breivik, K., Wania, F., 2002. Mass budgets, pathways and equilibrium states of two hexachlorocyclohexane in the Baltic Sea environment. Environ. Sci. Technol. 36, 1024–1032.

Dachs, J., Eisenreich, S.J., Baker, J.E., Ko, F., Jeremiason, J.D., 1999. Coupling of phytoplankton uptake and air–water exchange of persistent organic pollutants. Environ. Sci. Technol. 33, 3653–3660.

Dachs, J., Eisenreich, S.J., Hoff, R.M., 2000. Influence of eutrophication on air–water exchange, vertical fluxes, and phytoplankton concentrations of persistent organic pollutants. Environ. Sci. Technol. 34, 1095–1102.

Dachs, J., Lohmann, R., Ockenden, W.A., Mejanelle, L., Eisenreich, S.J., Jones, K.C., 2002. Oceanic biogeochemical controls on global dynamics of persistent organic pollutants. Environ. Sci. Technol. 36, 4229–4237.

Guglielmo, F., Lammel, G., Maier-Reimer, E., 2009. Global environmental cycling of DDT and γ-HCH in the 1980s: a study using a coupled atmosphere and ocean general circulation model. Chemosphere 76, 1509–1517.

Guglielmo, F., Stemmler, I., Lammel, G., 2012. The impact of organochlorines cycling in the cryosphere on their global distribution and fate −1. Sea ice. Environ. Pollut. 162, 475–481.

Guo, X., Hukuda, H., Miyazawa, Y., Yamagata, T., 2003. A triply nested ocean model for simulating the Kuroshio-roles of horizontal resolution on JEBAR. J. Phys. Oceanogr. 33, 146–169.

Ilyina, T., Pohlmann, T., Lammel, G., Sundermann, J., 2006. A fate and transport ocean model for persistent organic pollutants and its application to the North Sea. J. Mar. Syst. 63, 1–19.

Ilyina, T., Lammel, G., Pohlmann, T., 2008. Mass budgets and contribution of individual sources and sinks to the abundance of γ-HCH, α-HCH and PCB 153 in the North Sea. Chemosphere 72, 1132–1137.

Iwata, H., Tanabe, S., Sakai, N., Tatsukawa, R., 1993. Distribution of persistent organochlorines in the oceanic air and surface seawater and the role of ocean on their global transport and fate. Environ. Sci. Tecnol. 27, 1080–1098.

Jaward, F.M., Zhang, G., Nam, J.J., Sweetman, A.J., Obbard, J.P., Kobara, Y., Jones, K.C., 2005. Passive air sampling of polychlorinated bipheneyls, organochlorine compounds, and polybrominated diphenyl ethers across Asia. Environ. Sci. Technol. 39, 8638–8645.

Jurado, E., Lohmann, R., Meijer, S., Jones, K.C., Simo, R., Dachs, J., 2004. Latitudinal and seasonal capacity of the surface oceans as a reservoir of polychlorinated biphenyls. Environ. Pollut. 128, 149–162.

Jurado, E., Jaward, F., Lohmann, R., Jones, K.C., Simo, R., Dachs, J., 2005. Wet deposition of persistent organic pollutants to the global oceans. Environ. Sci. Technol. 33, 2426–2435.

Jurado, E., Zaldivar, J.M., Marinov, D., Dachs, J., 2007. Fate of persistent organic pollutants in the water column: does turbulent mixing matter? Mar. Pollut. Bull. 54, 441–451.

Kawai, T., Handoh, I.C., Takahashi, S., 2009. The rise of the Finely-Advanced Transboundary Environmental model (FATE): a state-of-the-art model prediction of the global sink of persistent organic pollutants. Organohalogen Compd. 71, 1610–1615.

Lohmann, R., Jurado, E., Pilson, M.E.Q., Dachs, J., 2006. Oceanic deep water formation as a sink of persistent organic pollutants. Geophys. Res. Lett. 33, L12607. http://dx.doi.org/10.1029/2006GL02593.

Lohmann, R., Breivik, K., Dachs, J., Muir, D., 2007. Global fate of POPs: current and future research directions. Environ. Pollut. 150, 150–165.

Meijer, S.N., Dachs, J., Fernandes, P., Camarero, L., Catalan, J., Vento, S.D., Drooge, B.V., Jurado, E., Grimalt, J.O., 2006. Modelling the dynamics air–water-sediment coupled fluxes and occurrence of polychlorinated biphenyls in a high altitude lake. Environ. Pollut. 140, 546–560.

Meijer, S.N., Grimalt, J.O., Fernandes, P., Dachs, J., 2009. Seasonal fluxes and temperature-dependent accumulation of persistent organic pollutants in lakes: the role of internal biogeochemical cycling. Environ. Pollut. 157, 1815–1822.

Mellor, G.L., 2003. Users guide for a three-dimensional, primitive equation, numerical ocean model (2003 version). Report, Program in Atmos. and Ocean Sci., Princeton Univ., Princeton, NJ, pp. 53.

Mellor, G.L., Yamada, T., 1982. Development of a turbulence closure model for geophysical fluid problem. Rev. Geophys. 20, 851–875.

Park, S., Chu, P.C., Lee, J.-H., 2011. Interannual-to-interdecadal variability of the Yellow Sea Cold Water Mass in 1967–2008: characteristics and seasonal forcings. J. Mar. Syst. 87, 177–193.

Schenker, U., Scheringer, M., Hungerbühler, K., 2008. Investigating the global fate of DDT: model evaluation and estimation of future trends. Environ. Sci. Tecnol. 42, 1178–1184.

Smagorinsky, J., 1963. General circulation experiments with the primitive equations: Part I. The basic experiment. Mon. Wea. Rev. 91, 99–164.

Smolarkiewicz, P.K., 1984. A fully multidimensional positive definite advection algorithm with small implicit diffusion. J. Comput. Phys. 54, 325–362.

Stemmler, I., Lammel, G., 2009. Cycling of DDT in the global environment 1950–2002: world ocean returns the pollutant. Geophys. Res. Lett. 36, L24602. http://dx.doi.org/10.1029/2009GL041340.

Stemmler, I., Lammel, G., 2010. Pathways of PFOA to the arctic: variabilites and contributions of oceanic currents and atmospheric transport and chemistry sources. Atmos. Chem. Phys. 10, 9965–9980.

Tanabe, S., Tatsukawa, R., 1983. Vertical transport and residence time of chlorinated hydrocarbons in the open ocean water column. J. Oceanogr. Soc. Jpn. 39, 53–62.

Ueno, D., Takahashi, S., Tanaka, H., Subramanian, A., Fillmann, G., Nakata, H., Lam, P.K., Zheng, J., Muchtar, M., Prudente, M., Chung, K.H., Tanabe, S., 2003. Global pollution monitoring of PCBs and organochlorine pesticides using skipjack tuna as a bioindicator. Arch. Environ. Contam. Toxicol. 45 (3), 378–389.

Wania, F., Axelman, J., Broman, D., 1998. A review of processes involved in the exchange of persistent organic pollutants across the air–Sea interface. Environ. Pollut. 102, 3–24.

Wania, F., Broman, D., Axelman, J., Naf, C., Agrell, C., 2001. A multicompartment, multi-basin fugacity model describing the fate of PCBs in the Baltic Sea. In: Wulff, F.V., Rahm, L.A., Larsson, P. (Eds.), A Systems Analysis of the Baltic Sea. Springer-Verlag, Berlin Heidelberg, pp. 417–448.

Supplementary material

Appendix A

On the basis of the biochemical processes in Fig. 1b, B_I in Eqs. (1) to (4) for C_W, C_{WPS}, C_{WPM}, and C_{WD} can be formulated as follows:

$$B_I(C_W) = -F_{WPS} - F_{WPM} + \phi_D C_{WD} - t_{1/2}^{-1} C_W, \tag{A.1}$$

$$B_I(C_{WPS}) = F_{WPS} - \phi_M C_{WPS}, \tag{A.2}$$

$$B_I(C_{WPM}) = F_{WPM} - \phi_M C_{WPM}, \tag{A.3}$$

$$B_I(C_{WD}) = \phi_M C_{WPM} + \phi_M C_{WPS} - \phi_D C_{WD} \tag{A.4}$$

Here, F_{WPS} (pg m^{-3} s^{-1}) is uptake between the water and the phytoplankton surface; F_{WPM} (pg m^{-3} s^{-1}) is uptake between the water and the phytoplankton matrix; ϕ_D (s^{-1}) is the decomposition rate of detritus-bound POPs; ϕ_M (s^{-1}) is the mortality rate of phytoplankton-bound POPs; and $t_{1/2}$ (s) is the half-life time of dissolved POPs.

We incorporated the water-phytoplankton (surface and matrix) exchange process following Dachs et al. (1999). The phytoplankton uptake in this study can be described as follows:

$$F_{WPS} = (k_{su} B_P C_W - k_{sd} C_{WPS}) \times \frac{1}{86400}, \quad F_{WPM} = (k_u B_P C_W - k_d C_{WPM}) \times \frac{1}{86400} \tag{A.5}$$

where B_P (kg m^{-3}) is phytoplankton biomass, k_{su} (m^3 kg^{-1} day^{-1}) is the uptake constant for the phytoplankton surface, k_u (m^3 kg^{-1} day^{-1}) is the uptake constant for the phytoplankton matrix, k_{sd} (day^{-1}) is the depuration constant for the phytoplankton surface, and k_d (day^{-1}) is the depuration constant for the phytoplankton matrix. Equations and parameters in the uptake/depuration processes are summarized in Supplementary Tables 1 and 2.

To include the degradation process of dissolved POPs by photolysis and biodegradation, we used the half-life time of POPs in Eq. (A.1). To represent the natural mortality process (ϕ_M s^{-1}) of phytoplankton-bound POPs, we used a formulation and parameters from Sohma et al. (2004):

$$\phi_M = \alpha_1 \exp(\beta_1 T) \times \frac{1}{86400} \tag{A.6}$$

where α_1 (= 0.00042 day^{-1}) is the phytoplankton mortality rate at 0 °C, β_1 (= 0.0693 $°C^{-1}$) is the temperature coefficient for phytoplankton mortality, and T is temperature (°C). A proportion of the detritus-bound POPs is transformed into POPs in water by decomposition. The decomposition process (ϕ_D, s^{-1}) of detritus-bound POPs was assumed to be dependent on temperature following Kawamiya et al. (1995):

$$\phi_D = \alpha_2 \exp(\beta_2 T) \times \frac{1}{86400} \tag{A.7}$$

where α_2 (= 0.03 day^{-1}) is the detritus decomposition rate at 0 °C, and β_2 (= 0.0693 $°C^{-1}$) is the temperature coefficient for detritus decomposition, and T is temperature (°C). The sinking velocity (w_{sp} m s^{-1}) of phytoplankton-bound POPs was assumed to be constant vertically, and was set to be 1/86400 m s^{-1} (1 m day^{-1}). Following Kawamiya et al. (1995), the sinking velocity (w_{sd} m s^{-1}) of detritus-bound POPs was set to be 10/86400 m s^{-1} (10 m day^{-1}) in the upper 100 m layer, and 100/86400 m s^{-1} (100 m day^{-1}) in the region deeper than 170 m. Between 100 m and 170 m, a linear relation between sinking velocity and depth was assumed. We used a half-life time of PCB 153, $t_{1/2} = 4.32 \times 10^8$ (s), given by Sinkkonen and Paasivirta (2000) for the degradation process of dissolved PCB 153.

In order to include the phytoplankton uptake process, the vertical distributions of phytoplankton biomass (B_P kg m^{-3} in Eq. (A.5)) are calculated by a constant weight ratio (Riemann

et al., 1989):

$$B_P = \frac{100}{3.03} \times Chl \times 10^{-6}, \tag{A.8}$$

where Chl (mg m^{-3}) is the vertical distribution of chlorophyll a concentration calculated by the Gaussian model (Siswanto et al., 2006) from monthly averaged observed data of chlorophyll a concentration at the surface from the Sea-viewing Wide Field-of-view Sensor (Sea WiFS). It must be noted that the weight ratio used in Eq. (A.8) has been suggested to vary seasonally (Riemann et al., 1989) and spatially (Chang et al., 2000). The usage of Eq. (A.8) excludes such temporal and spatial variations in the weight ratio but makes model results easily understood. As an example of monthly phytoplankton biomass, we describe the features of the surface chlorophyll a in winter and summer in Appendix B.1.

Appendix B

B.1 Physical and biological environments in the East China Sea

As an example of monthly phytoplankton biomass, we here describe the features of the surface chlorophyll a in winter and summer. In February, the surface chlorophyll a concentration is high along the coasts from 30 to 35°N on the Chinese side of the ECS and in the Bohai Sea, but is low in the Yellow Sea (Supplementary Fig. 1a). In August, the distribution of surface chlorophyll a is similar to that in February, but its concentration becomes low (Supplementary Fig. 1b).

To calculate k_{AW} (Supplementary Table 3), we used wind speed data from the European Remote-Sensing satellites ERS−1 and ERS−2. Since the net flux of POPs between air and water is affected by wind speed and water temperature, their spatial distributions in February and August, as examples, are shown in Supplementary Figs. 1c to 1f. In February, the whole area of the ECS is dominated by northerly winds with speeds larger than 5 m s^{-1} and is covered

by water with temperatures lower than 16 °C. In particular, the water temperature is very low in the Bohai and Yellow Seas. In August, southeasterly winds are dominant over the ECS, but the wind speeds are smaller than 4 m s^{-1} and water temperature is high over the whole ECS.

B.2 Key process responsible for seasonal variability in PCB 153

To elucidate the most important factor controlling the seasonal variability in PCB 153, we designed three sensitivity experiments in each of which the temporal variation of one parameter was removed while that of the others was kept. Specifically, we removed the temporal variation in chlorophyll *a* concentration (chlorophyll-run), wind speed (wind-run), and water temperature (temperature-run), respectively. The calculated monthly volume-averaged dissolved and particulate PCB 153 in each sensitivity experiments are shown in Supplementary Fig. 2. The detailed explanations are mentioned in text.

We next examined impacts of the seasonal variation in chlorophyll *a*, wind speed, and water temperature on the mass budget of PCB 153 (Supplementary Fig. 3). The removal of seasonal variation in water temperature and in wind speed reduces the annual surface flux by 45% and 22%, respectively, compared with the control-run. As a result of the decrease in surface flux, the mass flow associated with the other processes also decreases. For example, the reduction in phytoplankton uptake in the temperature-run is ∼40%. Thus, phytoplankton uptake-induced depletion of the dissolved PCB 153 partly contributes to the decrease of surface flux. In contrast, the mass balance in the chlorophyll-run is similar to that in the control-run, as suggested in Supplementary Fig. 2. This is because the supply of gaseous PCB 153 by the diffusive air-water exchange flux is controlled primarily by water temperature and secondly by wind speed.

B.3 Other processes affecting seasonal variability in PCB 153

In our simulation, the gaseous PCB 153 concentration was assumed to be constant throughout the year, meaning that gaseous PCB 153 concentration is not influenced by physical and biochemical processes in the ocean. However, the real concentration of PCB 153 in the atmosphere changes temporally. To examine impacts of gaseous PCB 153 concentration on the behavior of PCB 153 in the ocean, we conducted two additional numerical experiments. In the first numerical experiment, we carried out four simulations in which the gaseous PCB 153 concentration (2.08 pg m^{-3}) used in the control-run was multiplied by constants of 0.5, 2.0, 5.0, and 10.0, respectively. In the second numerical experiment, we also performed four simulations in which the gaseous PCB 153 concentration varies sinusoidally with a maximum value (3.08 pg m^{-3}) in February and a minimum value (1.08 pg m^{-3}) in August (winter-run), with a maximum in May and a minimum in November (spring-run), with a maximum in August and a minimum in February (summer-run), and with a maximum in November and a minimum in May (fall-run), while the yearly averaged concentration is the same as that (2.08 pg m^{-3}) in the control-run. In all simulations, the other boundary and initial conditions as well as the model integration period were the same as in the control-run. We compared the seasonal variability and biomass for the dissolved and particulate PCB 153 in the additional simulations with those in the control-run.

The first four simulations showed that the yearly averaged dissolved and particulate PCB 153 concentrations linearly changed in proportion to the gaseous PCB 153 concentration (Supplementary Fig. 4). To investigate the impact of the change in the supply of gaseous PCB 153 on the seasonal variation of dissolved and particulate PCB 153, we calculated a ratio of difference between the two extreme values of monthly mean to annual mean as a seasonal index of PCB 153. The ratios were 1.1 and 1.8 for the dissolved and particulate phases in the control-run,

respectively, and these two values did not change among the four simulations. These results indicate that a difference in the supply of gaseous PCB 153 is not important for the seasonal cycle in dissolved and particulate PCB 153 concentrations as long as the concentration is a constant value throughout the year.

From the second four simulations, the dissolved and particulate PCB 153 concentrations were high in winter and low in summer to fall (Supplementary Fig. 5a), regardless of the seasonal variation pattern in gaseous PCB 153 concentration. These are similar to results from the control-run. However, there is also an apparent difference in their seasonal variations. Concentration differences between the winter- or summer-runs and the control-run become large in January−June. This is partly because the winter-run in which gaseous PCB 153 concentration reaches a maximum in February increases the concentration gradient between the gaseous phase and the dissolved phase, resulting in increased surface flux (Supplementary Fig. 5b), while the summer-run, in which gaseous PCB 153 concentration reaches a minimum in February, decreases the concentration gradient between the gaseous phase and the dissolved phase, resulting in decreased surface flux (Supplementary Fig. 5b). From ratios of difference between the two extreme values of monthly mean to annual mean in each simulations (Supplementary Table 4), ratios in the spring- and fall-runs are found to be similar to those in the control-run. However, ratios in the winter-run are 1.3 and 2.1 for the dissolved and particulate phases, respectively, indicating larger seasonal variation, while those in the summer-run are 0.8 and 1.4, representing smaller seasonal variation. Such seasonal variations would be caused by the diffusive air-water exchange flux associated with the that in gaseous PCB 153. Thus a future model should incorporate the temporal variations in gaseous PCB 153 and its interaction with the PCB 153 in the ocean.

B.4 Simulations for different congeners of PCBs

For comparison with PCB 153, we conducted simulations for PCB 52, 101, and 180. Parameters used in simulations are shown in the Supplementary Table 5, but all other conditions are the same with those for PCB 153. The dissolved and particulate concentrations of PCB 52, 101, and 180 were high in winter and low in summer to fall (Supplementary Fig. 6), which are similar to the seasonal variation of PCB 153. However, there is a prominent difference in their amplitudes. This is due to the difference in the supply of gaseous concentration (Supplementary Table 5). It is also noted that the difference between PCB 52 and PCB 101 is considerably large in the dissolved concentration but small in the particulate concentration (Supplementary Figs. 6a and 6b). From the results of mass balance, the yearly integrated PCB 52, 101, and 180 from the atmosphere into the ocean are estimated to be 140.0, 74.7, and 41.0 kg year^{-1}, respectively (Supplementary Table 6). In the cases of PCB 101 and 180, the input from the atmosphere is removed by horizontal advection (57% and 55%) and sinking flux (39% and 44%), which are roughly the same as results for PCB 153. In the case of PCB 52, however, decomposition (8%) of the dissolved phase and advection (63%) are larger and sinking flux (28%) is smaller than those in the PCB 101 and 180. This is because PCB 52 has the shorter half-life time and has less hydrophobic property, compared with PCB 101 and 180.

References used in Supplementary material

Chang, J., Shiah, F.-K., Gong, G.-C., Chiang, K.P., 2003. Cross-shelf variation in carbon-to-chlorophyll *a* ratios in the East China Sea, summer 1998. Deep-Sea Res. II 50, 1237-1247.

Del Vento, S., Dachs, J., 2002. Prediction of uptake dynamics of persistent organic pollutants by bacteria and phytoplankton. Environ. Toxicol. Chem. 21, 941-953.

Jaward, F.M., Zhang, G., Nam, J.J., Sweetman, A.J., Obbard, J.P., Kobara, Y., Jones, K.C., 2005. Passive air sampling of polychlorinated bipheneyls, organochlorine compounds, and polybrominated diphenyl ethers across Asia. Environ. Sci. Technol. 39, 8638-8645.

Kawamiya, M., Kishi, J.M., Yamanaka, Y., Suginohara, N., 1995. An ecological-physical coupled model applied to Station Papa. J. Oceanogr. 51, 635-664.

Riemann, B., Simonsen, P., Stensgaard, L., 1989. The carbon and chlorophyll content of phytoplankton from various nutrient regimes. J. Plankton Res. 11, 1037-1045.

Sinkkonen, S., Paasivirta, J., 2000. Degradation half-life times of PCDDs, PCDFs and PCBs for environmental fate modeling. Chemosphere 40, 943-949.

Siswanto, E., Ishizaka, J., Yokouchi, K., 2006. Optimal primary production model and parameterization in the eastern East China Sea. J. Oceanogr. 62, 361-372.

Sohma, A., Sekiguchi, Y., Nakata, K., 2004. Modeling and evaluating the ecosystem of sea-grass beds, shallow waters without sea-grass, and an oxygen-depleted offshore area. J. Mar. Sys. 45, 105-142.

Supplementary Table 1: Physicochemical parameters in the water-phytoplankton exchange process (Vento and Dachs, 2002). See Supplementary Table 2 for water viscosity (η_H m^2 s^{-1}), octanol viscosity (η_P cP), and bioconcentration factors (BCF m^3 kg^{-1}).

Equations or parameters	Unit	Value	Description
$k_{su}(T) = \frac{\eta_H(298)}{\eta_H(T)} \frac{T}{298} k_{su}(298)$	m^3 kg^{-1} d^{-1}		Uptake constant of phytoplankton surface at T K for POPs
$k_{sd}(T) = \frac{\eta_H(298)}{\eta_H(T)} \frac{T}{298} \frac{BCF(298)}{BCF(T)} k_{sd}(298)$	d^{-1}		Depuration constant of phytoplankton surface at T K for POPs
$k_u(T) = \frac{\eta_P(298)}{\eta_P(T)} \frac{T}{298} \frac{BCF(T)}{BCF(298)} k_u(298)$	m^3 kg^{-1} d^{-1}		Uptake constant of phytoplankton matrix at T K for POPs
$k_d(T) = \frac{\eta_P(298)}{\eta_P(T)} \frac{T}{298} k_d(298)$	d^{-1}		Depuration constant of phytoplankton surface at T K for POPs
$k_{su}(298)$	m^3 kg^{-1} d^{-1}	110039	Uptake constant of phytoplankton surface at 298 K for PCB 153
$k_{sd}(298)$	d^{-1}	287.6	Depuration constant of phytoplankton surface at 298 K for PCB 153
$k_u(298)$	m^3 kg^{-1} d^{-1}	2474	Uptake constant of phytoplankton matrix at 298 K for PCB 153
$k_d(298)$	d^{-1}	1.08	Depuration constant of phytoplankton matrix at 298 K for PCB 153
T	K		Water temperature

Supplementary Table 2: Physicochemical parameters in the water-phytoplankton exchange process (Vento and Dachs, 2002). T (K) is water temperature.

Equations or parameters	Unit	Value	Description
$\frac{BCF}{BCF(298)} = \exp\left[\frac{\Delta H_S}{R}\left(\frac{1}{T} - \frac{1}{298}\right)\right]$			Bioconcentration factors (BCFs)
$BCF(298)$	$m^3\ kg^{-1}$	396 (1934)	BCFs for the surface (matrix) at 298 K for PCB 153
ΔH_S	$kJ\ mol^{-1}$	35	Enthalpy of sorption for POPs
R	$Pa\ m^3\ mol^{-1}\ K^{-1}$	8.31	Ideal gas constant
$\log_{10}\eta_H(T) = \frac{1301}{998.333+8.1855(T-293)+0.00585(T-293)^2}$			
-3.30233			Water viscosity for $273 < T < 293$
$\log_{10}\frac{\eta_H(T)}{\eta_H(293)} = \frac{1.3272(293-T)-0.001053(T-293)^2}{T-168}$			Water viscosity for $293 < T < 373$
$\eta_H(293)$	$m^2\ s^{-1}$	2.56×10^{-5}	Water viscosity at 293 K
$\eta_P^{-0.2661}(T) = \eta_P^{-0.2661}(298) + \frac{T-298}{233}$			Octanol viscosity at T K
$\eta_P(298)$	cP	7.21	Octanol viscosity at 298 K

Supplementary Table 3: Physicochemical parameters in the air-water exchange process (Bidleman and McConnell, 1995). T (K) is water temperature. R (Pa m^3 mol^{-1} K^{-1}) is the ideal gas constant given in Supplementary Table 2.

Equations or parameters	Unit	Value	Description
$1/k_{AW} = 1/k_W + 1/k_A H'$	m s^{-1}		Mass transfer coefficient between air and water
$k_W = 0.45 U_{10}^{1.64} \left(Sc_{POPs}/600 \right)^{-0.5}$	m s^{-1}		Mass transfer coefficient in water
$k_A = (0.2U_{10} + 0.3) \left(D_{POPs,a}/D_{H_2O,a} \right)^{0.61}$	m s^{-1}		Mass transfer coefficient in air
U_{10}	m s^{-1}		Wind speed at 10 m height
Sc_{POPs}		2780	Schmidt number for PCB 153
$D_{POPs,a}$	m^2 s^{-1}	5.2×10^{-6}	Molecular diffusivity for PCB 153
$D_{H_2O,a}$	m^2 s^{-1}	2.56×10^{-5}	Molecular diffusivity for H_2O
$\ln H' = -\Delta H_H/RT + \Delta S_H/R$			Henry's law constant
ΔH_H	kJ mol^{-1}	66.1	Enthalpy of phase change for PCB 153
ΔS_H	kJ mol^{-1} K^{-1}	0.19	Entropy of the phase change for PCB 153

Supplementary Table 4: Ratios of difference between the maximum and minimum value to the yearly-mean concentration in the dissolved (C_W) and particulate ($C_{WP} + C_{WD}$) PCB 153. The ctl denotes the control-run. For the definition of winter-, spring-, summer-, and fall-runs, refer to text.

	ctl	winter-run	spring-run	summer-run	fall-run
Ratio for the dissolved PCB 153	1.1	1.3	1.1	0.8	1.2
Ratio for the particulate PCB 153	1.8	2.1	1.9	1.4	2.0

Supplementary Table 5: Parameters used in simulations for PCB 52, 101, and 180. C_A (pg m^{-3}) is gaseous concentration (Jaward et al., 2006), $t_{1/2}$ ($\times 10^8$ s) is half-life time (Sinkkonen and Paasivirta, 2000), k_{su} (m^3 kg^{-1} day^{-1}) is the uptake constant for the phytoplankton surface, k_u (m^3 kg^{-1} day^{-1}) is the uptake constant for the phytoplankton matrix, k_{sd} (day^{-1}) is the depuration constant for the phytoplankton surface, and k_d (day^{-1}) is the depuration constant for the phytoplankton matrix (Vento and Dachs, 2002).

	C_A	$t_{1/2}$	k_{su}	k_u	k_{sd}	k_d
PCB52	10.10	1.08	82608	287.6	402.5	0.89
PCB101	4.68	2.16	121044	287.6	1559.0	1.15
PCB180	2.46	8.64	82000	287.6	1300.0	0.53

Supplementary Table 6: Yearly-integrated mass (kg year^{-1}) balances calculated by the model.

	PCB 52	PCB 101	PCB 180
Surface FLux	140.0	74.7	41.0
Sinkgin Flux	38.5	29.4	17.8
Decomposition of C_W	11.3	2.5	0.3
Decomposition of C_{WD}	2.9	2.9	2.0
Advection/Diffusion of C_W	87.4	40.9	21.5
Advection/Diffusion of C_{WP}	1.1	1.2	0.9
Advection/Diffusion of C_{WD}	0.2	0.3	0.2
Uptake-Depuration	42.7	33.6	20.9
C_W	38.8	1.7	0.1
C_{WP}	16.8	1.5	0.1
C_{WD}	8.4	1.0	0.1

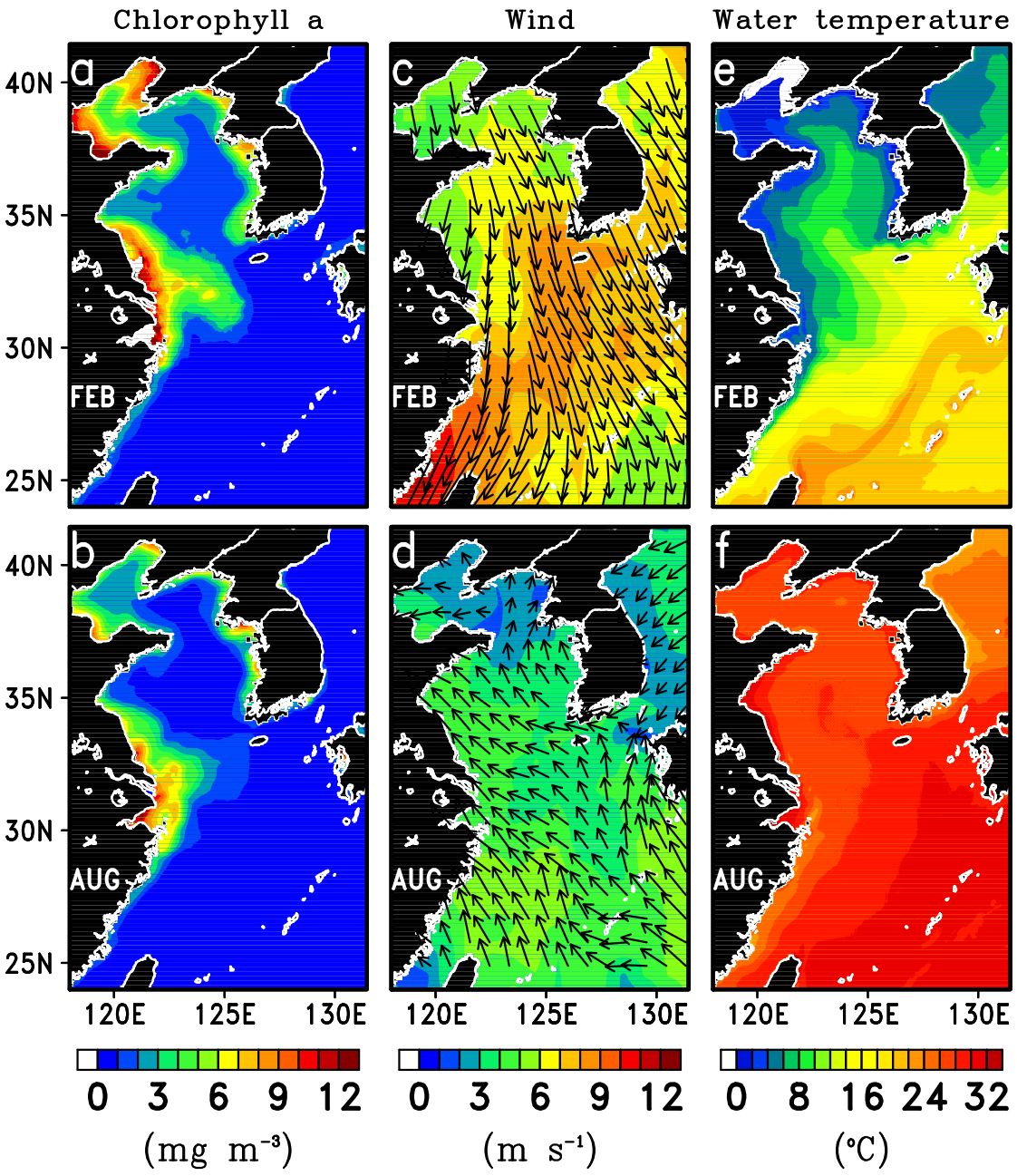

Supplementary Fig. 1: Horizontal distributions of monthly-averaged (a and b) surface chlorophyll *a* concentration, (c and d) wind speed and direction at 10 m height, and surface water temperature, in February and August, respectively.

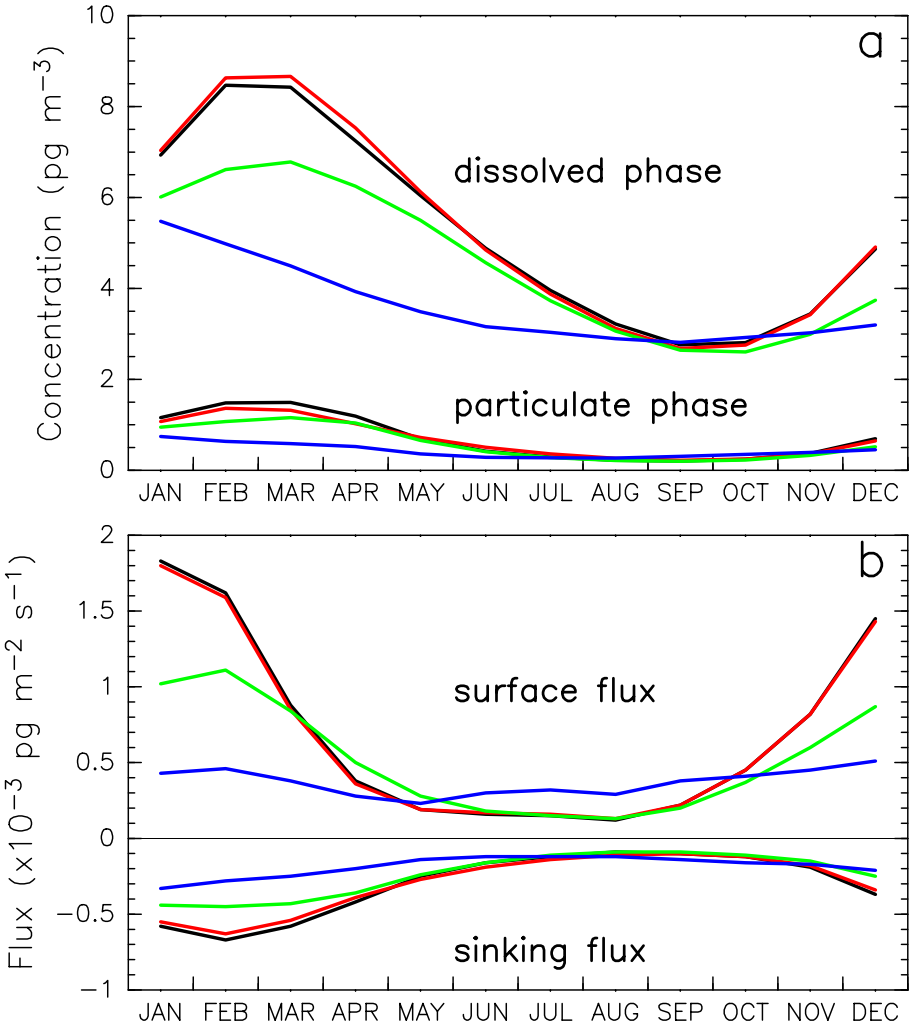

Supplementary Fig. 2: Time series of (a) monthly-averaged concentration in the dissolved and particulate PCB 153 and (b) surface and sinking fluxes, from control-run (black lines), chlorophyll-run (red lines), wind-run (green lines), and temperature-run (blue lines), respectively.

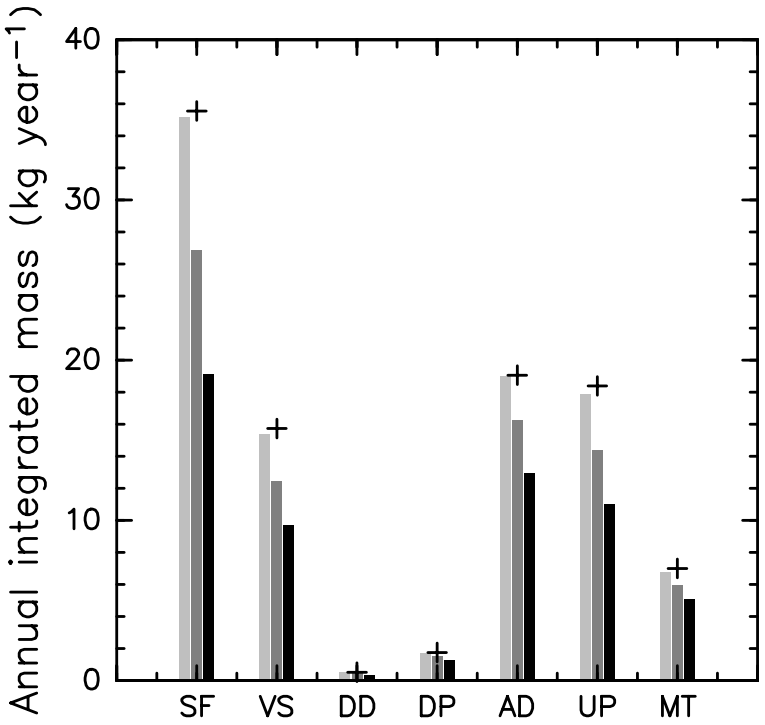

Supplementary Fig. 3: Yearly-integrated mass (kg year^{-1}) balances calculated by the model for the control-run (plus), chlorophyll-run (light-gray bar), wind-run (heavy-gray bar), and temperature-run (black), respectively. SF is yearly-integrated mass by surface flux of PCB 153 from the atmosphere to the ocean, VS is that by vertical sinking of PCB 153 to the bottom, DD is that by decomposition of dissolved PCB 153, DP is that by decomposition of phytoplankton-bound PCB 153, AD is that by advection/diffusion of dissolved and particulate PCB 153, UP is that by phytoplankton uptake, and MT is that by mortality of phytoplankton-bound PCB 153.

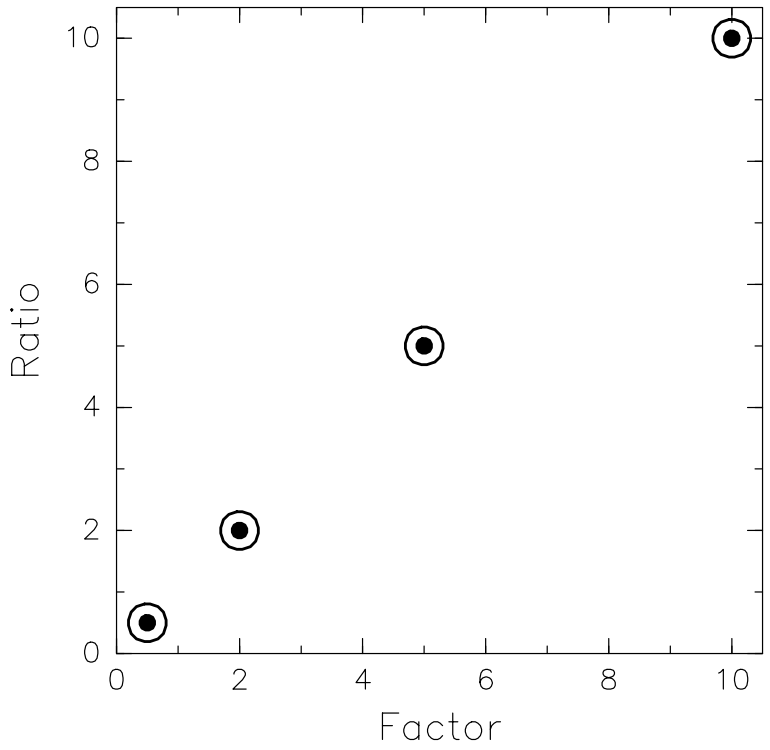

Supplementary Fig. 4: Ratio of the yearly-integrated concentrations in the dissolved (open circles) and particulate (black circles) PCB 153 in four sensitivity experiments to those in the control-run. Factor is a coefficient multiplied by the gaseous concentration (2.08 pg m^{-3}) used in the control-run.

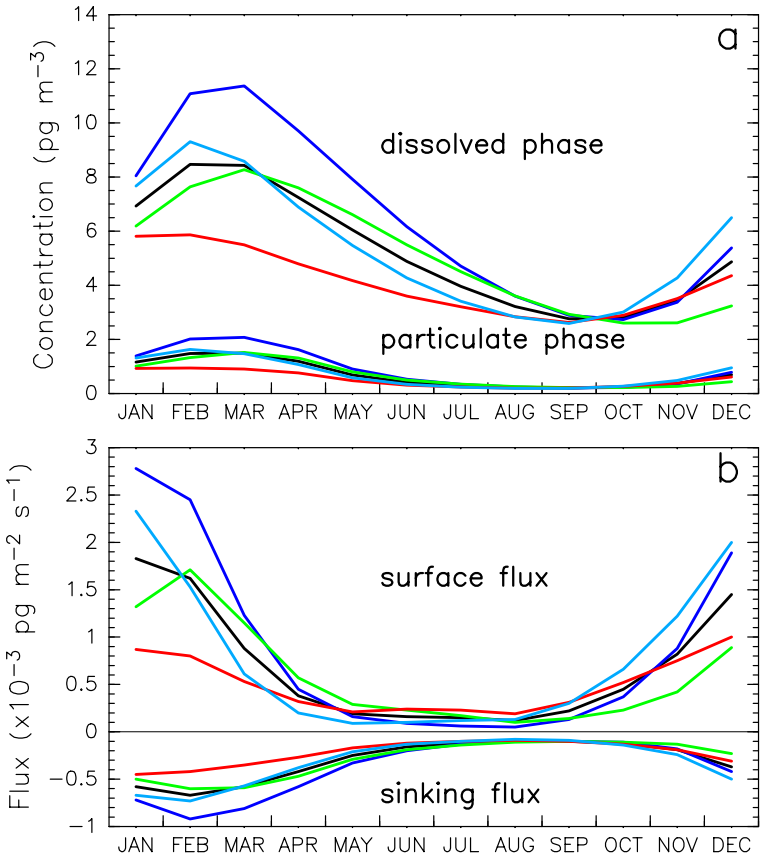

Supplementary Fig. 5: Similar to Supplementary Fig 4, but for the control-run (black lines),February-run (blue lines), May-run (green lines), August-run (red lines), and November-run (sky-blue lines), respectively.

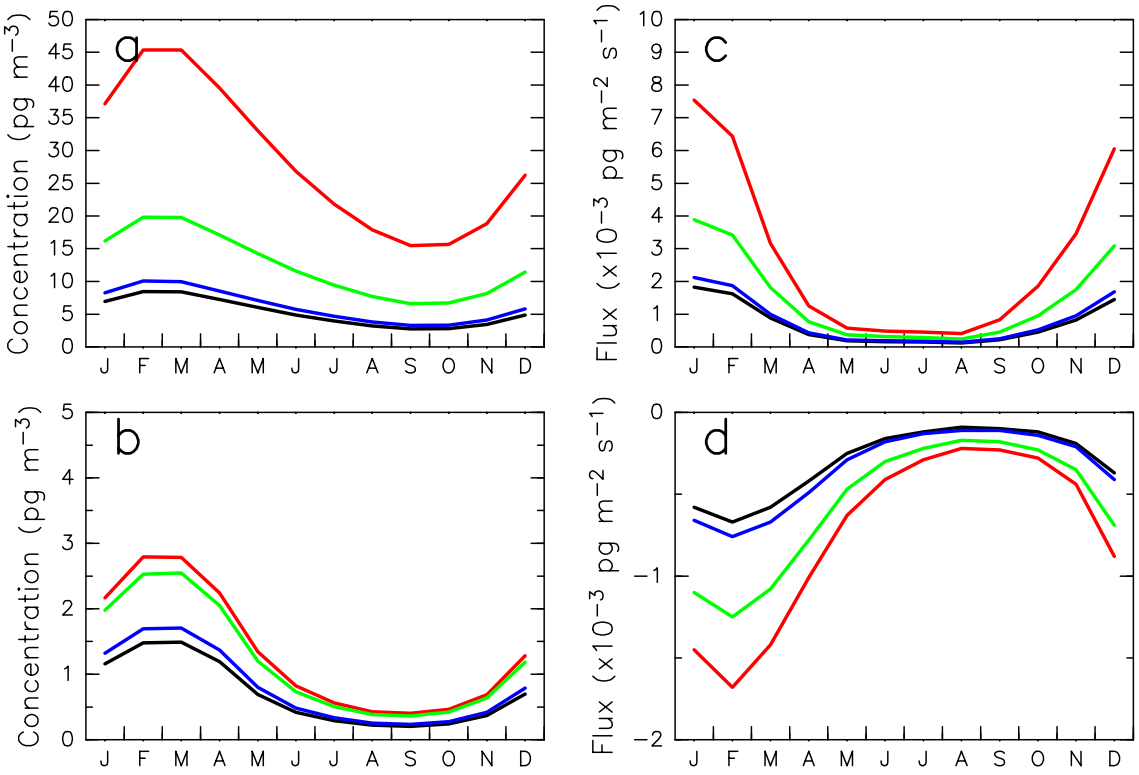

Supplementary Fig. 6: Time series of monthly-averaged (a) dissolved and (b) particulate concentrations and (c) surface and (d) sinking fluxes, for PCB 153 (black lines), 52 (red lines), 101 (green lines), and 180 (blue lines), respectively.